Post-fire behaviour and resistances of square recycled aggregate concrete-filled stainless steel tube stub columns

DOI:
10.1016/j.tws.2024.111564

Wang, Z.Y., Zhong, Y.K., Jiang K., Su, M., Zhao, O., (2024), "Post-fire behaviour and resistances of square recycled aggregate concrete-filled stainless steel tube stub columns", Thin-walled Structures, 197:111564.

Post-fire behaviour and resistances of square recycled aggregate concrete-filled stainless steel tube stub columns

Ziyi Wang [a], Yukai Zhong [b,*], Ke Jiang [a, c], Meini Su [d], Ou Zhao [a,*]

[a] School of Civil and Environmental Engineering, Nanyang Technological University, Singapore

[b] Research Center for Wind Engineering and Engineering Vibration, Guangzhou University, Guangzhou, China

[c] Department of Civil and Natural Resources Engineering, University of Canterbury, Christchurch, New Zealand

[d] School of Engineering, The University of Manchester, Manchester, UK

[*] Corresponding author, Email: yukai.zhong@gzhu.edu.cn (Yukai Zhong), ou.zhao@ntu.edu.sg (Ou Zhao)

Abstract: Experimental and numerical studies on the cross-section compressive behaviour and residual resistances of square recycled aggregate concrete-filled stainless steel tube (RACFSST) stub columns after exposure to fire are reported in this paper. An experimental programme was firstly carried out on twelve stub column specimens with three recycled coarse aggregate replacement ratios (0%, 35% and 70%) after exposure to the ISO-834 standard fire for 0 min (i.e. at ambient temperature), 15 min, 30 min and 45 min. The test results, including load–end shortening curves, failure loads and failure modes, were presented, with the initial compressive stiffness and confinement effect analysed. The experimental programme was followed by a numerical modelling programme, where thermal and mechanical finite element models were developed and validated against the test results and afterwards used to conduct parametric studies to generate additional numerical data over a wide range of cross-section dimensions. Based on the test and numerical data, the relevant design rules for square natural aggregate concrete-filled carbon steel tube stub columns at ambient temperature, as specified in the European code, Australia/New Zealand standard and American specification, were evaluated, using post-fire material properties, for their applicability to square RACFSST stub columns after exposure to fire. The evaluation results generally revealed that the European code and Australian/New Zealand standard led to a good level of design accuracy, while the American specification resulted in slightly conservative post-fire cross-section compression resistance predictions.

Keywords: Design analyses; ISO-834 standard fire; Numerical modelling; Post-fire cross-section compression resistances; Square RACFSST stub columns; Recycled aggregate concrete; Thermal and mechanical analyses

1. Introduction

Due to the acceleration of urbanisation in recent decades, the massive consumption of natural resources and growing demands of landfills for construction wastes have led to a global focus on construction sustainability. One effective way to achieve sustainability in the construction industry is to reuse construction and demolition wastes. Recycled aggregate concrete (RAC), with natural coarse aggregates partially or fully replaced by recycled coarse aggregates, is regarded as a representative and promising example of waste reuse [1, 2]. However, to date, the use of RAC is only limited to non-load-bearing (non-structural) members in engineering applications, such as pavements and infill walls, due to its lower compressive strength and ductility compared with natural aggregate concrete (NAC) [2–4]. The application of RAC could be potentially broadened to load-bearing (structural) members by introducing it in the concrete-filled steel tube (CFST) composite structure system, by means of which the strength and ductility of RAC can be significantly improved due to the favourable confinement provided by the outer steel tube to the inner concrete core.

Experimental and numerical studies on recycled aggregate concrete-filled steel tube (RACFST) members have been previously carried out, with a brief review summarised herein. Axial compression tests were conducted on RACFST stub columns with circular [5–9], square [8–11] and rectangular [10, 11] sections to investigate their cross-section compressive behaviour and resistances, with the influence of recycled coarse aggregate (RCA) replacement ratios discussed, codified design rules evaluated and modified design approaches proposed. The improvement of strength and ductility of RAC in the CFST composite structure system was verified through circular RACFST beam and beam-column tests by Chen et al. [12], while Yang and Han [13] experimentally investigated the flexural buckling behaviour of circular and square RACFST columns and beam-columns and highlighted the slightly inferior resistances of RACFST columns compared with those columns with NAC infills. With regards to the RACFST stub columns after exposure to fire, Li et al. [14] and Yang and Hou [15] conducted axial compression tests to study their post-fire structural behaviour and resistances, highlighted the negative effect of elevated temperature on the strength and stiffness of RACFST stub columns and proposed new design formulae.

It should be noted that the abovementioned studies were all conducted on RACFST members with outer tubes made of carbon steels. However, the severe corrosion issue of carbon steels not only makes their maintenance costly, but also threatens the safety of structural members. Therefore, the use of stainless steel tubes in replacement of carbon steel tubes in CFST, namely recycled aggregate concrete-filled stainless steel tube (RACFSST), has gained increasing attention from researchers and engineers, due to the excellent corrosion-resistant nature as well as favourable material properties (e.g., higher strength and ductility) of stainless steels. Currently, studies on RACFSST members remain scarce, with only limited research conducted on RACFSST columns [16–20] and beams [17] at ambient temperature. Fire is known to pose a significant risk to the safety of steel and steel–concrete composite structures. However, to date, there are no investigations into RACFSST members in and after exposure to fire.

This paper reports experimental and numerical investigations into the cross-section compressive behaviour and residual resistances of square RACFSST stub columns after exposure to fire. An experimental programme, including heating of specimens, cylinder tests as well as post-fire tensile coupon tests and stub column tests, was firstly conducted. Twelve square RACFSST stub column specimens, designed with three RCA replacement ratios (0%, 35% and 70%), were tested at ambient temperature and after exposure to the ISO-834 standard fire [21] for 15 min, 30 min and 45 min. Subsequently, a numerical modelling programme was performed, where thermal and mechanical finite element models were developed and validated against the test results and then used to perform parametric studies to generate further numerical data. Given the absence of design standards for RACFSST composite structures after exposure to fire, the relevant design rules for square natural aggregate concrete-filled carbon steel tube (NACFCST) stub columns at ambient temperature, as specified in EN 1994-1-1 [22], AS/NZS 2327 [23] and ANSI/AISC 360-16 [24], were evaluated, using post-fire material properties, for their applicability to square RACFSST stub columns after exposure to fire, based on the test and numerical data.

2. Experimental programme

2.1 Specimens

The experimental programme adopted nine square RACFSST stub column specimens after exposure to fire and three reference specimens at ambient temperature. The twelve specimens were fabricated from cold-formed grade MT-304 austenitic stainless steel [25] square hollow section SHS 120 × 120 × 5 (labelled as S120) and three types of concretes R0, R35 and R70 (denoting concretes with RCA replacement ratios of 0%, 35% and 70%, respectively), leading to three specimen series, namely S120-R0, S120-R35 and S120-R70. Each specimen series included four specimens, with one reference specimen at ambient temperature and three specimens after exposure to the ISO-834 standard fire [21] for 15 min, 30 min and 45 min. The label of each specimen included the identifier of the specimen series and a letter 'T' followed by the corresponding heating duration, e.g., S120-R35-T45. Table 1 reports the measured geometric dimensions of each square RACFSST stub column specimen, including the outer cross-section width b, outer cross-section depth h, wall thickness t, inner corner radius r_i (see Fig. 1) and member length L, as well as the RCA replacement ratio r and heating duration T_h.

Three types of coarse aggregates, including single-sized recycled coarse aggregates with a nominal size of 20 mm, single-sized natural coarse aggregates with a nominal size of 8 mm and graded natural coarse aggregates with continuous sizes from 5 mm to 20 mm, were used to produce the recycled and natural aggregate concretes. The physical properties of each type of coarse aggregates, including the loose mass density, apparent particle density and water absorption ratio, were measured according to BS EN 1097-3 [26] and BS EN 1097-6 [27] and are summarised in Table 2. The actual particle size distribution for each type of the recycled and natural coarse aggregates was measured using the sieving method prescribed in BS EN 933-1 [28], with the grading curves shown in Fig. 2, where the percentages passing by mass are plotted against the sieve sizes of 2.5 mm, 5 mm, 10 mm, 20 mm, 31.5 mm and 40 mm. The requirements for the Grading Category G_c80/20 of BS EN 12620 [29] are reported in Table 3 and displayed as an envelope in Fig. 2. The mixture proportions of the three types of concretes are summarised in Table 4, with the resulting grading curves all lying within the grading envelope and shown in Fig. 2. Note that prior to concrete casting, the recycled coarse aggregates were sun-dried and then pre-wetted by adding additional water based on the water absorption ratios reported in Table 2, in order to compensate for the high water absorption of recycled coarse aggregates and achieve the same effective water-to-cement ratio for the three types of concretes [3, 19, 20].

2.2 Heating of specimens

For each heating duration, the corresponding square RACFSST stub column specimens, together with a bare stainless steel tube (for cutting coupons), were heated in an electric furnace (see Fig. 3), where a series of heating elements are uniformly distributed over both sides of the chamber and capable of providing heating according to the ISO-834 standard fire curve. Prior to heating, both ends of each specimen were welded with steel plates, to prevent the inner concrete core from explosive spalling during heating. Note that no preloads were applied to the specimens during heating, which would result in lower residual resistances than those heated with preloading [30–32]. Upon attainment of the pre-specified heating duration T_h, the furnace was turned off to let the specimens naturally cool down to the ambient temperature and then the welded end plates were removed from the specimens.

For each heating duration, four thermocouples were used to measure the thermal responses (temperature–time histories) of the outer stainless steel tube and inner concrete core of a representative specimen at the mid-height. The arrangement of the thermocouples at the mid-height cross-section is shown in Fig. 4, where one thermocouple is attached to the outer surface of the stainless steel tube (denoted as Point 4) and three thermocouples are inserted into the inner concrete core at different points (denoted as Points 1–3). Fig. 5 shows the measured temperature–time curves for each heating duration, together with the heating curve measured from the temperature probe of the furnace, while the corresponding maximum temperatures of Points 1–4 (denoted as T_1, T_2, T_3 and T_4, respectively) are reported in Table 5. Fig. 6 displays the surface colours of the inner concrete cores of a typical specimen series S120-R35 after exposure to fire, showing increasing light-grey as the heating durations increase.

2.3 Material testing

Flat and corner tensile coupons were cut from the corresponding bare stainless steel tubes after exposure to fire, with their locations shown in Fig. 1 and geometric dimensions satisfying the requirements of ASTM E8/E8M-15a [33]. The surface colours of the grade MT-304 austenitic stainless steel become champagne gold, dark blue and dark grey for the heating durations of 15 min, 30 min and 45 min, respectively – see Fig. 7. Note that the change of surface colour results from the fact that oxide layers with different thicknesses are formed for different elevated temperatures during heating [34–36] and later reflect light with different wavelengths at ambient temperature. Tensile coupon tests were conducted by using a displacement-controlled Schenck 250 kN tensile testing machine, with displacement rates set as 0.05 mm/min and 0.8 mm/min before and after attainment of the nominal 0.2% proof stresses. The tensile coupon test setup is displayed in Fig. 8, with an extensometer installed over the central 50 mm of the coupon to measure the elongations during testing and two strain gauges attached to the mid-height of the coupon to record the longitudinal strains. Fig. 9 shows the measured flat and corner stress–strain curves of the austenitic stainless steel SHS 120 × 120 × 5 tubes at ambient temperature and after exposure to the ISO-834 standard fire for different heating durations. The key measured ambient temperature material properties are reported in Table 6(a), where E is the Young's modulus, $\sigma_{0.2}$ is the 0.2% proof stress, σ_u is the ultimate stress, ε_u is the strain at the ultimate stress, ε_f is the strain at fracture and n and m are the strain hardening exponents used in the Ramberg–Osgood material model [37], while the post-fire material properties, denoted with an additional subscript 'T', are summarised in Table 6(b).

For each of the three types of concretes (R0, R35 and R70), ten concrete cylinders were cast and cured together with the corresponding square RACFSST stub column specimens, with four of them tested at 28 days after casting and the other six tested on the same day of the stub column tests. The concrete cylinder test setup is shown in Fig. 10, where two strain gauges are attached to the concrete cylinder to measure the compressive strains. A constant loading rate of 0.6 MPa/s was used for the concrete cylinder tests. Note that concrete cylinder tests were only conducted at ambient temperature due to the fact that unconfined concrete cylinders are prone to explosive spalling when exposure to fire. Upon completion of concrete cylinder tests, the secant moduli of concretes were determined based on the strain gauge data and the method specified in BS EN 12390-13 [38]. For each type of concrete, the average measured 28-day compressive strength $f_{c,28}$ is reported in Table 7, together with the average compressive strength f_c and secant modulus E_{cm} measured on the same day of the stub column tests.

2.4 Stub column tests

Compression tests were carried out on the twelve square RACFSST stub column specimens to study their cross-section compressive behaviour and residual resistances after exposure to fire. A displacement-controlled Instron 5000 kN hydraulic testing machine was employed to conduct stub column tests with the displacement rate set as 0.3 mm/min. Prior to testing, each end of the specimens was milled flat and covered with a thin layer of high strength gypsum, to ensure a uniform distribution of stresses on each specimen end during testing. Fig. 11 shows the stub column test setup, where four strain gauges are attached to the mid-height of the specimen to record both the longitudinal and circumferential strains and four LVDTs are vertically located at the upper platen of the testing machine to measure the end shortenings.

The measured load–end shortening curves for each series of the square RACFSST stub column specimens at ambient temperature and after exposure to fire are displayed in Fig. 12. The key measured test results of the specimens at ambient temperature, including the failure load N_u, the end shortening at the failure load δ_u and the initial compressive stiffness EA, which is taken as the secant stiffness at $0.4N_u$ [39], are reported in Table 8(a), while the test results of the specimens after exposure to fire (denoted with an additional subscript 'T'), together with the $N_{u,T}/N_u$ and $(EA)_T/(EA)$ ratios, are summarised in Table 8(b). The failure modes of three typical specimens S120-R0-T15, S120-R35-T15 and S120-R70-T15 are displayed in Fig. 13, featuring outward buckling of the outer stainless steel tubes coupled with crushing of the inner concrete cores.

It can be seen from Fig. 12 that although axial deformation increases rapidly at the post-ultimate load stage, no sudden drops of loads are observed, which can be mainly attributed to the beneficial confinement effect. Fig. 14 displays the development of the circumferential-to-longitudinal strain ratios $\varepsilon_{ci}/\varepsilon_l$ for a typical specimen series S120-R35, evidencing that (i) the initial values of the $\varepsilon_{ci}/\varepsilon_l$ ratios for different heating durations are around 0.3, which is the Poisson's ratio of stainless steel and (ii) the onset of confinement effect (where the $\varepsilon_{ci}/\varepsilon_l$ ratios start to deviate from 0.3) for specimens with longer heating duration is earlier.

The influence of heating duration on the initial compressive stiffness is evaluated in Fig. 15, where the $(EA)_T/(EA)$ ratios for each specimen series are plotted against the heating durations, while the influence of RCA replacement ratio on the initial compressive stiffness can be assessed based on the values of $(EA)_T$ in Table 8. The following conclusions can be drawn: (i) for the specimens with the same RCA replacement ratio, the extent of reduction in initial compressive stiffness increases as the heating duration increases and (ii) for the specimens with the same heating duration, the initial compressive stiffness decreases with the RCA replacement ratio. The influences of heating duration and RCA replacement ratio on the failure load are evaluated in Fig. 16 and Fig. 17, respectively, with the results revealing that (i) the failure loads of the square RACFSST stub column specimens with the same RCA replacement ratios show relatively evident reductions for heating durations of 30 min and 45 min and (ii) for the specimens with the same heating durations, the failure loads decrease as the RCA replacement ratios increase.

3. Numerical modelling

3.1 General

Following the laboratory testing, numerical modelling was performed by using the general-purpose finite element (FE) analysis software ABAQUS [40]. Two types of FE models, namely thermal and mechanical FE models, were respectively developed to simulate the test thermal (temperature–time) responses of the square RACFSST stub column specimens when exposure to fire and their test structural (load–end shortening) responses after exposure to fire. The developed thermal and mechanical FE models were validated against the corresponding test results and then used to perform parametric studies to generate further numerical data over a wide range of cross-section dimensions.

3.2 Development and validation of thermal FE models

The four-node shell heat transfer element DS4 [40] and eight-node brick heat transfer element DC3D8 [40] have been successfully used to model thermal responses of concrete-filled steel tube members [41–44] and were also adopted herein. Based on a mesh sensitivity study evaluating element sizes from $(b+h)/80$ to $(b+h)/20$, the final element sizes for both the DS4 and DC3D8 elements were taken as $(b+h)/40$. The thermal properties of stainless steel, including the density, thermal conductivity and specific heat, were determined in accordance with EN 1993-1-2 [45], while the thermal properties of concretes were determined according to EN 1994-1-2 [46], with the specific heat revised by taking the moisture content as 5% of the weight [43, 47]. Note that the thermal expansion coefficients of concretes and stainless steel were omitted, with the density kept constant when exposure to fire. The emissivity and heat transfer coefficient were respectively taken as 0.2 and 35 W/m^{2}K [48], to consider the heat radiation and convection between the outer surface of the stainless steel tube and the surrounding environment. Due to the distinct difference in thermal expansion properties between the outer stainless steel tube and inner concrete core, an air gap was generated at their interface during heating and heat transfer was allowed for through gap conductance with the coefficient taken as 100 W/m^{2}K [42–44].

Upon development of the thermal FE models, the temperature–time curves measured from the outer surfaces of the stainless steel tubes (at Point 4 – see Fig. 4) were assigned to the outer surfaces of the corresponding square RACFSST stub column FE models. Subsequently, heat transfer analyses were conducted to obtain the numerical thermal (temperature–time) responses. The accuracy of the developed thermal FE models was evaluated through graphical and quantitative comparisons between the experimental and numerical thermal responses of the inner concrete cores. Table 9 reports the comparisons between the experimental and numerical maximum temperatures at Points 1–3 of the inner concrete cores (see Fig. 4), revealing good agreement. Fig. 18 shows the experimental and numerical temperature–time curves at the three measured positions of the inner concrete core for a typical specimen S120-R35-T45, indicating that the experimental temperature–time curves can be well simulated by their numerical counterparts. To conclude, the developed thermal FE models were capable of accurately replicating the experimental thermal responses of the square RACFSST stub column specimens when exposure to the ISO-834 standard fire and hence regarded as validated.

3.3 Development and validation of mechanical FE models

The four-node shell element S4R [40] and eight-node brick element C3D8R [40] have been widely used to simulate structural responses of recycled aggregate concrete-filled stainless steel tube members [16, 19, 20] and were also adopted herein. To keep consistency with the element size of the thermal FE models, $(b+h)/40$ was chosen as the element size for both the S4R and C3D8R elements. Regarding the material modelling of the outer stainless steel tubes at ambient temperature and after exposure to fire, the measured (engineering) stress–strain curves from the tensile coupon tests were firstly converted into the true stress–plastic strain curves and then inputted into the plastic material model [40]. The Poisson's ratio of the outer stainless steel tubes was set as 0.3. The concrete damage plasticity (CDP) model [40] was employed for the material modelling of the inner concrete cores at ambient temperature and after exposure to fire. For each type of concrete at ambient temperature, the Poisson's ratio was set as 0.2 and the secant modulus was taken as the measured value reported in Table 7, while the material plastic parameters in the CDP model were determined based on the recommendations of Tao et al. [49]. For each type of concrete after exposure to fire, the residual compressive strength $f_{c,T}$ and the strain at the residual compressive strength $\varepsilon_{c,T}$ were determined according to the suggestions of Song et al. [31] and Yang et al. [32] and the post-fire secant modulus was taken as $4700f_{c,T}^{0.5}$ [50], based on which other material plastic parameters in the CDP model can be calculated. To consider the beneficial confinement provided by the outer stainless steel tubes on the inner concrete cores, equivalent uniaxial compressive stress–strain curves, as determined in accordance with the recommendations of Han et al. [51] and further revised to account for the influence of the RCA replacement ratio [4], were inputted into the CDP model. With regards to the tensile stress–strain relationship, it was assumed to be linear elastic up to the concrete tensile strength of $0.1f_c$ (or $0.1f_{c,T}$), followed by the inelastic post-ultimate material response, characterised by means of the fracture energy G_F [52].

The surface-to-surface contact was used to model the interaction between the outer stainless steel tube and inner concrete core. Specifically, a hard contact was adopted to simulate the behaviour in the normal direction, while a penalty method was employed to represent the tangential behaviour, with the friction coefficient set as 0.25. To model the test fixed-ended boundary conditions, each end section of the square RACFSST stub column FE models was coupled to a concentric reference point, with only longitudinal translation of one reference point allowed and other degrees of freedom restrained.

Upon development of the mechanical FE models, nonlinear analyses were carried out to obtain the numerical failure loads, load-end shortening curves and failure modes. The accuracy of the developed mechanical FE models was then evaluated against the test results. Table 8 reports the numerical to experimental failure load ratios for all the square RACFSST stub column specimens, indicating good agreement. Comparisons between the experimental and numerical load–end shortening curves for three typical specimens S120-R0-T15, S120-R35-T15 and S120-R70-T15 are displayed in Fig. 19, where the overall shapes and peak loads of the experimental load–deformation curves are well captured by their numerical counterparts. Good agreement between the experimental and numerical failure modes is also evident in Fig. 13. In summary, the developed mechanical FE models can accurately simulate the experimental mechanical responses of the square RACFSST stub column specimens after exposure to fire and were thus regarded as validated.

3.4 Parametric studies

Based on the validated thermal and mechanical FE models, parametric studies were performed to generate additional numerical data over a wide range of cross-section dimensions. Specifically, the outer cross-section depths and widths of modelled square stainless steel tubes were set as 120 mm, 150 mm and 200 mm. The wall thicknesses were chosen between 2.0 mm and 8.0 mm, leading to both non-slender and slender cross-sections to be considered, while the inner corner radii were set as 1.5 times the corresponding wall thicknesses. The member length of each modelled square RACFSST stub column was taken as three times the outer cross-section depth. Three types of concretes, including two types of RACs (R35 and R70) and one type of NAC (R0), were considered in the parametric studies. For each modelled square RACFSST stub column, four fire exposure conditions were considered, including at ambient temperature and after exposure to the ISO-834 standard fire for 15 min, 30 min and 45 min. The geometric dimensions of the outer stainless steel tubes, together with the types of the inner concrete cores and the heating durations selected for parametric studies, are summarised in Table 10. Finally, a total of 72 numerical data on square RACFSST stub columns after exposure to fire were generated.

4. Evaluation of design standards

4.1 General

Given that there are no existing design codes for RACFSST members after exposure to fire, the relevant design rules for square NACFCST stub columns at ambient temperature, as set out in EN 1994-1-1 [22], AS/NZS 2327 [23] and ANSI/AISC 360-16 [24], were evaluated, using post-fire material properties, for their applicability to square RACFSST stub columns after exposure to fire. To consider the uneven temperature field of the inner concrete core, it was discretised into five layers with equal thickness, with the maximum attained temperature of each layer during heating taken as that at the mid-point of the layer. The post-fire compressive strength $f_{c,T,i}$ of each layer was then determined from Eq. (1) [46], where $k_{c,T,max}$ is the strength reduction factor and dependent on the maximum attained temperature T_{max} during heating. The final design post-fire compressive strength of the whole inner concrete core $f_{c,w,T}$ was calculated as the weighted average (by area) post-fire compressive strength from all the five layers. The post-fire 0.2% proof stress $\sigma_{0.2,T}$ of each outer stainless steel tube was taken as the weighted average (by area) 0.2% proof stress from both flat and corner regions.

$$f_{c,T,i} = f_c \begin{cases} k_{c,T,\max} & 20\ ^\circ\mathrm{C} \le T_{\max} < 100\ ^\circ\mathrm{C} \\ 1.0 - \left[0.235 \times \left(T_{\max} - 100\right)/200\right] & 100\ ^\circ\mathrm{C} \le T_{\max} < 300\ ^\circ\mathrm{C} \\ 0.9 k_{c,T,\max} & T_{\max} \ge 300\ ^\circ\mathrm{C} \end{cases} \qquad (1)$$

4.2 EN 1994-1-1 (EC4)

The design cross-section compression resistance of a square NACFCST stub column at ambient temperature, as specified in the European code EN 1994-1-1 [22], is determined as the summation of the resistances of the outer steel tube and inner concrete core, as given in Eq. (2), where f_y is the yield stress of the outer carbon steel tube, A_c is the gross cross-section area of the inner concrete core and A_s is taken as the gross cross-section area if the cross-section of the outer carbon steel tube is non-slender but the effective cross-section area if the cross-section of the outer carbon steel tube is slender. The effective cross-section area is calculated based on the effective width method, with the EC4 reduction factor for slender plate element ρ_{EC4} determined from Eq. (3), where $\bar{\lambda}_{EC4}$ is the EC4 plate element slenderness and given by Eq.

(4), in which $\varepsilon = \sqrt{235/f_y}$ is the material parameter, $k_\sigma = 10.67$ is the buckling coefficient for plate elements of CFST with only outward buckling [53] and $c_{EC4} = h - 3t$ or $c_{EC4} = b - 3t$ is the EC4 flat element width.

$$N_{u,EC4} = A_s f_y + A_c f_c \tag{2}$$

$$\rho_{EC4} = \frac{\bar{\lambda}_{EC4} - 0.22}{\bar{\lambda}_{EC4}^2} \leq 1.0 \quad \text{for } \bar{\lambda}_{EC4} > 0.673 \tag{3}$$

$$\bar{\lambda}_{EC4} = \frac{c_{EC4}/t}{28.3\varepsilon\sqrt{k_\sigma}} \tag{4}$$

The EC4 residual cross-section compression resistances of square RACFSST stub columns after exposure to fire were calculated from Eqs (2)–(4), but with f_c and f_y replaced by the corresponding post-fire material properties $f_{c,w,T}$ and $\sigma_{0.2,T}$. A quantitative evaluation of the EC4 predicted failure loads is reported in Table 11, with the overall mean ratio of the test and FE to EC4 predicted failure loads $N_{u,T}/N_{u,T,EC4}$ (or $N_u/N_{u,EC4}$) and the corresponding COV respectively equal to 1.14 and 0.11. The test and FE to EC4 predicted failure load ratios $N_{u,T}/N_{u,T,EC4}$ (or $N_u/N_{u,EC4}$) are plotted against the EC4 flat element width-to-thickness ratios c_{EC4}/t, as shown in Fig. 20. The quantitative and graphical evaluation results revealed that the combined use of the EC4 ambient temperature design rules and post-fire material properties generally resulted in accurate failure load predictions for square RACFSST stub columns after exposure to fire.

4.3 AS/NZS 2327 (AS/NZS)

The Australian/New Zealand standard AS/NZS 2327 [23] employs the same design approach to determine the cross-section compression resistance of a square NACFCST stub column at ambient temperature as that specified in EN 1994-1-1 [22], with the only difference lying in the reduction factor. The AS/NZS reduction factor is determined from Eq. (5), where $\lambda_{AS/NZS}$ is the AS/NZS plate element slenderness, as given by Eq. (6), in which $c_{AS/NZS} = h - 2t$ or $c_{AS/NZS} = b - 2t$ is the AS/NZS flat element width.

$$\rho_{AS/NZS} = \frac{64}{\lambda_{AS/NZS}} \leq 1.0 \quad (5)$$

$$\lambda_{AS/NZS} = \frac{c_{AS/NZS}}{t}\sqrt{\frac{f_y}{250}} \quad (6)$$

The AS/NZS residual cross-section compression resistances of square RACFSST stub columns after exposure to fire were calculated based on the combined use of the ambient temperature design rules and post-fire material properties. Quantitative and graphical comparisons between the AS/NZS predicted failure loads and the test and FE failure loads were then made. Table 11 reports the mean test and FE to AS/NZS predicted failure load ratios $N_{u,T}/N_{u,T,AS/NZS}$ (or $N_u/N_{u,AS/NZS}$) and the corresponding COVs, while the $N_{u,T}/N_{u,T,AS/NZS}$ (or $N_u/N_{u,AS/NZS}$) ratios are plotted against the $c_{AS/NZS}/t$ ratios and displayed in Fig. 21, both indicating relatively accurate failure load predictions for square RACFSST stub columns after exposure to fire.

4.4 ANSI/AISC 360-16 (AISC)

The American specification ANSI/AISC 360-16 [24] classifies the outer carbon steel tube sections of square NACFCST members into compact, non-compact and slender cross-sections by comparing the AISC flat element width-to-thickness ratios with the slenderness limits. The AISC flat element width-to-thickness ratio λ_{AISC} is calculated as $\lambda_{AISC} = c_{AISC}/t$, where $c_{AISC} = h - 2t - 2r_i$ or $c_{AISC} = b - 2t - 2r_i$ is the AISC flat element width, while the slenderness limits for compact/non-compact cross-sections and non-compact/slender cross-sections are respectively taken as $\lambda_p = 2.26\sqrt{E / f_y}$ and $\lambda_r = 3.00\sqrt{E / f_y}$. Upon completion of the cross-section classification, the cross-section compression resistances of square NACFCST stub columns at ambient temperature are calculated by Eqs. (7)–(9) for compact, non-compact and slender tube sections, respectively, where f_{cr} is the design failure stress of the outer carbon steel tube and given by Eq. (10).

$$N_{u,AISC} = f_y A_s + 0.85 f_c A_c \quad \text{for } \lambda_{AISC} < \lambda_p \tag{7}$$

$$N_{u,AISC} = f_y A_s + 0.85 f_c A_c - \frac{0.15 f_c A_c}{\left(\lambda_r - \lambda_p\right)^2}\left(\lambda_{AISC} - \lambda_p\right)^2 \quad \text{for} \quad \lambda_p,, \lambda_{AISC} < \lambda_r \tag{8}$$

$$N_{u,AISC} = f_{cr} A_s + 0.7 f_c A_c \quad \text{for } \lambda_{AISC} .. \lambda_r \tag{9}$$

$$f_{cr} = \frac{9E}{\left(c_{AISC} / t\right)^2} \tag{10}$$

On the basis of the combined use of the ambient temperature design rules and post-fire material properties, the AISC residual cross-section compression resistances of square RACFSST stub columns after exposure to fire were determined and then evaluated against the test and FE failure loads. Table 11 reports the mean ratios of the test and FE to AISC predicted failure loads $N_{u,T}/N_{u,T,AISC}$ (or $N_u/N_{u,AISC}$) and the corresponding COVs, revealing that the AISC ambient temperature design rules combined with the post-fire material properties led to slightly conservative failure load predictions for square RACFSST stub columns after exposure to fire. The same conclusion can be drawn from the graphical evaluation results shown in Fig. 22, where the $N_{u,T}/N_{u,T,AISC}$ (or $N_u/N_{u,AISC}$) ratios are plotted against the c_{AISC}/t ratios.

5. Conclusions

The post-fire cross-section compressive behaviour and resistances of square RACFSST stub columns have been investigated through testing and numerical modelling. The experimental programme included compression tests on twelve square RACFSST stub column specimens at ambient temperature and after exposure to the ISO-834 standard fire for 15 min, 30 min and 45 min. The influences of heating duration and RCA replacement ratio on the initial compressive stiffness and confinement effect were discussed. The test results were used in the numerical modelling programme to validate the developed thermal and mechanical FE models, which were then employed to conduct parametric studies to generate additional numerical data. Given the lack of design codes for RACFSST composite structures after exposure to fire, the relevant design rules for square NACFCST stub columns at ambient temperature were evaluated, using post-fire material properties, for their applicability to square RACFSST stub columns after exposure to fire. It can be concluded that the combined use of the EC4 or AS/NZS ambient temperature design rules and post-fire material properties resulted in accurate residual cross-section compression resistance predictions for square RACFSST stub columns after exposure to fire, while the AISC design rules combined with the post-fire material properties provided slightly conservative design.

Acknowledgements

The present research work is financially supported by the Singapore Ministry of Education Academic Research Fund (AcRF) Tier 1 Grant (Award Number: RG122/21) and the National Natural Science Foundation of China (NSFC) (Grant Number: 52308158). The recycled coarse aggregates used in the present research were sponsored by Pan-United Corporation Ltd.

References

[1] Tam, V. W., Soomro, M. and Evangelista, A. C. J. (2018). A review of recycled aggregate in concrete applications (2000–2017). Construction and Building Materials, 172, 272-292.

[2] de Andrade Salgado, F. and de Andrade Silva, F. (2022). Recycled aggregates from construction and demolition waste towards an application on structural concrete: A review. Journal of Building Engineering, 52, 104452.

[3] Chen, Z., Xu, J., Chen, Y. and Lui, E. M. (2016). Recycling and reuse of construction and demolition waste in concrete-filled steel tubes: A review. Construction and Building Materials, 126, 641–660.

[4] Xiao, J., Li, J. and Zhang, C. (2005). Mechanical properties of recycled aggregate concrete under uniaxial loading. Cement and Concrete Research, 35(6), 1187-1194.

[5] de Azevedo, V. D. S., de Lima, L. R., Vellasco, P. C. D. S., Tavares, M. E. D. N. and Chan, T. M. (2021). Experimental investigation on recycled aggregate concrete filled steel tubular stub columns under axial compression. Journal of Constructional Steel Research, 187, 106930.

[6] Xiao, J., Huang, Y., Yang, J. and Zhang, C. (2012). Mechanical properties of confined recycled aggregate concrete under axial compression. Construction and Building Materials, 26(1), 591–603.

[7] Wang, Y., Chen, J. and Geng, Y. (2015). Testing and analysis of axially loaded normal-strength recycled aggregate concrete filled steel tubular stub columns. Engineering Structures, 86, 192–212.

[8] Lyu, W. Q., Han, L. H. and Hou, C. (2021). Axial compressive behaviour and design calculations on recycled aggregate concrete-filled steel tubular (RAC-FST) stub columns. Engineering Structures, 241, 112452.

[9] Yang, Y. and Han, L. (2006). Compressive and flexural behaviour of recycled aggregate concrete filled steel tubes (RACFST) under short-term loadings. Steel and Composite Structures, 6(3), 257.

[10] Yang, D., Liu, F. and Wang, Y. (2023). Axial compression behaviour of rectangular recycled aggregate concrete-filled steel tubular stub columns. Journal of Constructional Steel Research, 201, 107687.

[11] Yang, Y. F., Hou, C. and Liu, M. (2021). Tests and numerical simulation of rectangular RACFST stub columns under concentric compression. Structures, 27, 396-410.

[12] Chen, J., Wang, Y., Roeder, C. W. and Ma, J. (2017). Behavior of normal-strength recycled aggregate concrete filled steel tubes under combined loading. Engineering Structures, 130, 23–40.

[13] Yang, Y. F. and Han, L. H. (2006). Experimental behaviour of recycled aggregate concrete filled steel tubular columns. Journal of Constructional Steel Research, 62(12), 1310-1324.

[14] Li, W., Luo, Z., Tao, Z., Duan, W. H. and Shah, S. P. (2017). Mechanical behavior of recycled aggregate concrete-filled steel tube stub columns after exposure to elevated temperatures. Construction and Building Materials, 146, 571-581.

[15] Yang, Y. F. and Hou, R. (2012). Experimental behaviour of RACFST stub columns after exposed to high temperatures. Thin-Walled Structures, 59, 1-10.

[16] Tam, V. W., Wang, Z. B. and Tao, Z. (2014). Behaviour of recycled aggregate concrete filled stainless steel stub columns. Materials and Structures, 47(1), 293–310.

[17] Yang, Y. F. and Ma, G. L. (2013). Experimental behaviour of recycled aggregate concrete filled stainless steel tube stub columns and beams. Thin-Walled Structures, 66, 62–75.

[18] Zhang, W. H., Wang, R., Zhao, H., Lam, D. and Chen, P. (2022). Axial-load response of CFST stub columns with external stainless steel and recycled aggregate concrete: Testing, mechanism analysis and design. Engineering Structures, 256, 113968.

[19] Zhong, Y., Zhao, O. and Young, B. (2022). Experimental and numerical investigations of recycled aggregate concrete-filled stainless steel tube stub columns under combined compression and bending. Engineering Structures, 266, 114502.

[20] He, A., Su, A., Liang, Y. and Zhao, O. (2021). Experimental and numerical investigations of circular recycled aggregate concrete-filled stainless steel tube columns. Journal of Constructional Steel Research, 179, 106566.

[21] ISO 834, Fire-resistance Tests—Elements of Building Construction—Part 1: General Requirements, ISO 834-1, International Organization for Standardization, Geneva, Switzerland, 1999.

[22] EN 1994-1-1, Eurocode 4: Design of Composite Steel and Concrete Structures – Part 1-1: General Rules and Rules for Buildings, European Committee for Standardization (CEN), Brussels, 2004.

[23] Australian/New Zealand Standards, Composite structures—Composite steel-concrete construction in buildings. AS/NZS 2327-2017, Sydney, Australia, 2017.

[24] American Institute of Steel Construction (AISC). Specification for structural steel buildings. AISC 360-16, Chicago (IL); 2016.

[25] ASTM A554, Standard specification for welded stainless steel mechanical tubing, Pennsylvania, USA, American Society for Testing and Materials, 2021.

[26] BS EN 1097-3, Tests for Mechanical and Physical Properties of Aggregates - Part 3: Determination of Loose Bulk Density and Voids, European Committee for Standardization (CEN), Brussels, 1998.

[27] BS EN 1097-6, Tests for Mechanical and Physical Properties of Aggregates - Part 6: Determination of Partical Density and Water Absorption, European Committee for Standardization (CEN), Brussels, 2022.

[28] BS EN 933-1, Tests for Geometrical Properties of Aggregates - Part 1: Determination of Particle Size Distribution - Sieving Method, European Committee for Standardization (CEN), Brussels, 2012.

[29] BS EN 12620, Aggregates for Concrete, European Committee for Standardization (CEN), Brussels, 2015 [Draft for public comment].

[30] Huo, J., Huang, G. and Xiao, Y. (2009). Effects of sustained axial load and cooling phase on post-fire behaviour of concrete-filled steel tubular stub columns. Journal of Constructional Steel Research, 65(8-9), 1664-1676.

[31] Song, T. Y., Han, L. H. and Yu, H. X. (2010). Concrete filled steel tube stub columns under combined temperature and loading. Journal of Constructional Steel Research, 66(3), 369-384.

[32] Yang, H., Han, L. H. and Wang, Y. C. (2008). Effects of heating and loading histories on post-fire cooling behaviour of concrete-filled steel tubular columns. Journal of Constructional Steel Research, 64(5), 556-570.

[33] American Society for Testing and Materials (ASTM), Standard Test Methods for Tension Testing of Metallic Materials. E8/E8M-15a, ASTM International, West Conshohocken, PA, USA, 2015.

[34] Wang, X. Q., Tao, Z., Song, T. Y. and Han, L. H. (2014). Stress–strain model of austenitic stainless steel after exposure to elevated temperatures. Journal of Constructional Steel Research, 99, 129-139.

[35] Cao, G., Firouzdor, V., Sridharan, K., Anderson, M. and Allen, T. R. (2012). Corrosion of austenitic alloys in high temperature supercritical carbon dioxide. Corrosion Science, 60, 246–255.

[36] Ziemniak, S. E. and Hanson, M. (2002). Corrosion behavior of 304 stainless steel in high temperature, hydrogenated water. Corrosion Science, 44(10), 2209–2230.

[37] Arrayago, I., Real, E. and Gardner, L. (2015). Description of stress–strain curves for stainless steel alloys. Materials & Design, 87, 540–552.

[38] BS EN 12390-13:2013, Testing Hardened Concrete – Part 13: Determination of Secant Modulus of Elasticity in Compression, European Committee for Standardization (CEN), Brussels, 2013.

[39] Wang, Z. B., Tao, Z., Han, L. H., Uy, B., Lam, D. and Kang, W. H. (2017). Strength, stiffness and ductility of concrete-filled steel columns under axial compression. Engineering Structures, 135, 209-221.

[40] Karlsson Hibbitt, Inc Sorensen, ABAQUS/Standard user's Manual Volumes I-III and ABAQUS CAE Manual. Version 6.14, Pawtucket (USA) 2014.

[41] Tao, Z. and Ghannam, M. (2013). Heat transfer in concrete-filled carbon and stainless steel tubes exposed to fire. Fire Safety Journal, 61, 1-11.

[42] Liu, F., Gardner, L. and Yang, H. (2014). Post-fire behaviour of reinforced concrete stub columns confined by circular steel tubes. Journal of Constructional Steel Research, 102, 82-103.

[43] He, A., Liang, Y. and Zhao, O. (2020). Behaviour and residual compression resistances of circular high strength concrete-filled stainless steel tube (HCFSST) stub columns after exposure to fire. Engineering Structures, 203, 109897.

[44] Zhong, Y. and Zhao, O. (2022). Concrete-filled high strength steel tube stub columns after exposure to fire: Testing, numerical modelling and design. Thin-Walled Structures, 177, 109428.

[45] EN 1993-1-2:2005. Eurocode 3: Design of steel structures – Part 1-2: General rules — Structural fire design. Brussels: European Committee for Standardization (CEN); 2005.

[46] EN 1994-1-2:2005+A1:2014. Eurocode 4: design of composite steel and concrete structures – Part 1-2: General rules – Structural fire design. Brussels: European Committee for Standardization (CEN); 2014.

[47] Lu, H., Zhao, X. L. and Han, L. H. (2008). Finite element analysis of temperatures in concrete filled double skin steel tubes exposed to fires. In 4th International Structural Engineering and Construction Conference, ISEC-4-Innovations in Structural Engineering and Construction (pp. 1151-1156).

[48] Gardner, L. and Ng, K. T. (2006). Temperature development in structural stainless steel sections exposed to fire. Fire Safety Journal, 41(3), 185-203.

[49] Tao, Z., Wang, Z. B. and Yu, Q. (2013). Finite element modelling of concrete-filled steel stub columns under axial compression. Journal of constructional steel research, 89, 121-131.

[50] American Concrete Institute, Building Code Requirements for Structural Concrete Vols. 318–14, ACI, Farmington Hills, MI, 2014.

[51] Han, L. H., Yao, G. H. and Tao, Z. (2007). Performance of concrete-filled thin-walled steel tubes under pure torsion. Thin-Walled Structures, 45(1), 24-36.

[52] CEB-FIP, Euro-International Committee for Concrete (CEB)-International Federation for Prestressing (FIP). Model Code for Concrete Structures (CEB-FIPMC 2010), Thomas Telford, London, U.K., 2010.

[53] Bradford, M. A., Wright, H. D. and Uy, B. (1998). Local buckling of the steel skin in lightweight composites induced by creep and shrinkage. Advances in Structural Engineering, 2(1), 25-34.

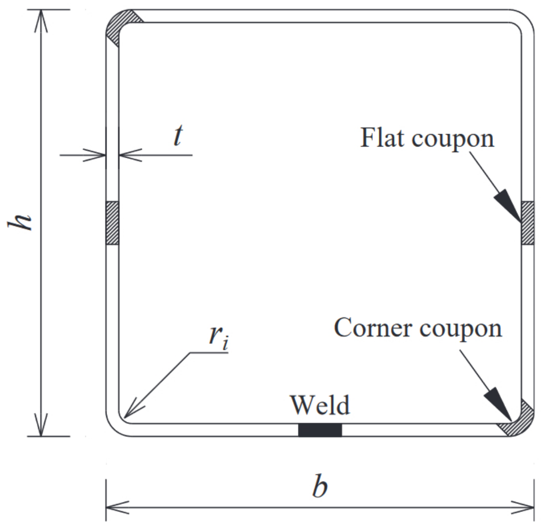

Fig. 1. Definition of cross-section geometric parameters and locations of coupons.

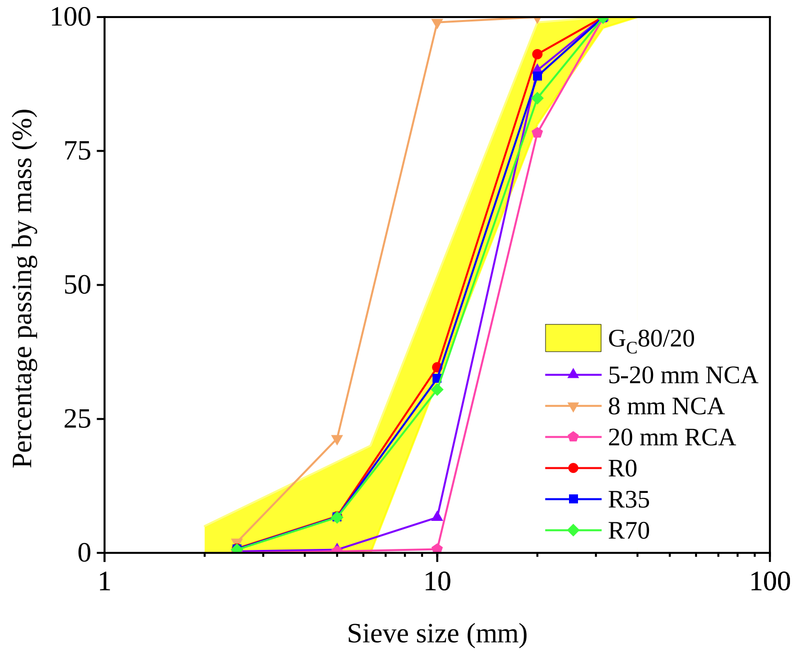

Fig. 2. Grading curves of coarse aggregates.

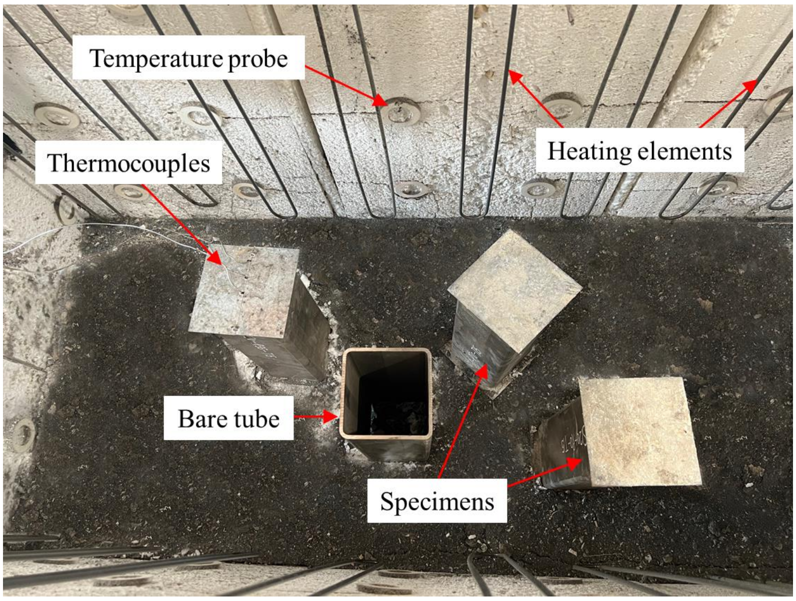

Fig. 3. Specimens heated in electric furnace and instrumentation.

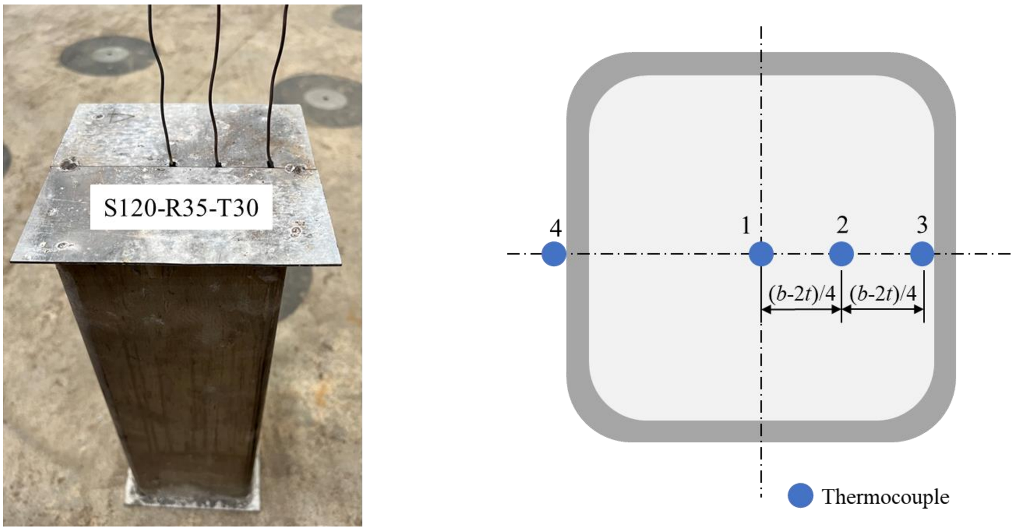

Fig. 4. Arrangement of thermocouples at mid-height cross-section.

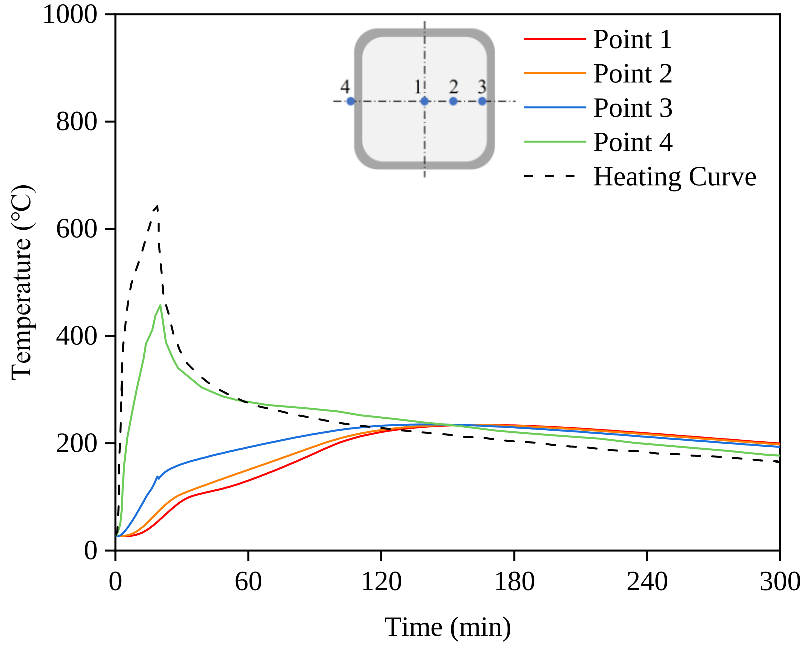

(a) S120-R35-T15

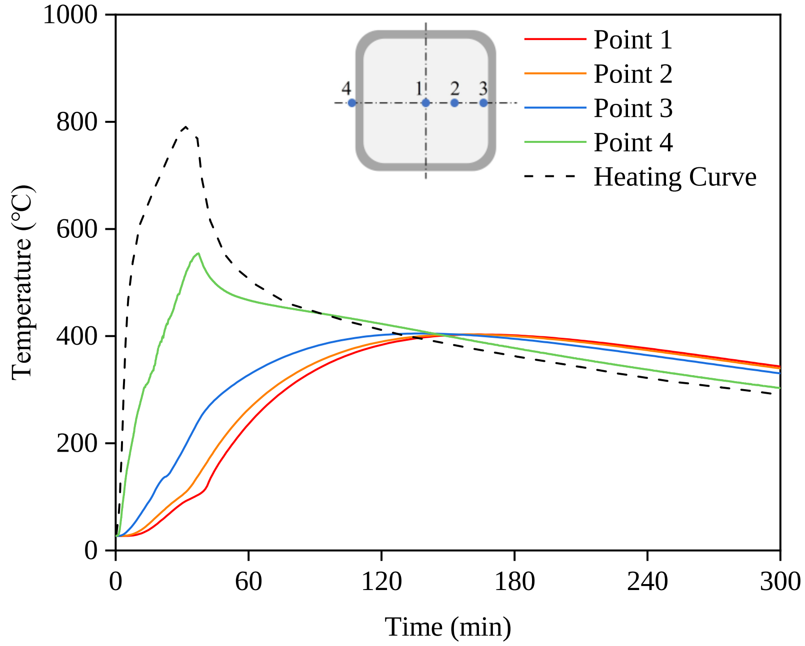

(b) S120-R35-T30

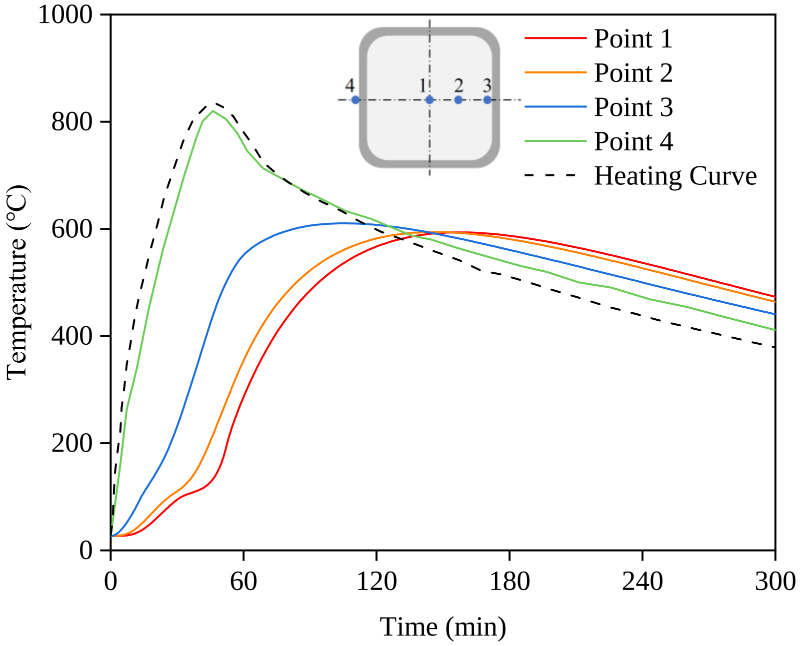

(c) S120-R35-T45

Fig. 5. Temperature–time curves measured from typical square RACFSST stub column specimen for each heating duration.


(a) T_h=0 min (b) T_h=15 min


(c) T_h=30 min (d) T_h=45 min

Fig. 6. Surface colours of inner concrete cores after exposure to fire for different heating durations.

Fig. 7. Surface colours of austenitic stainless steel after exposure to fire for different heating durations.

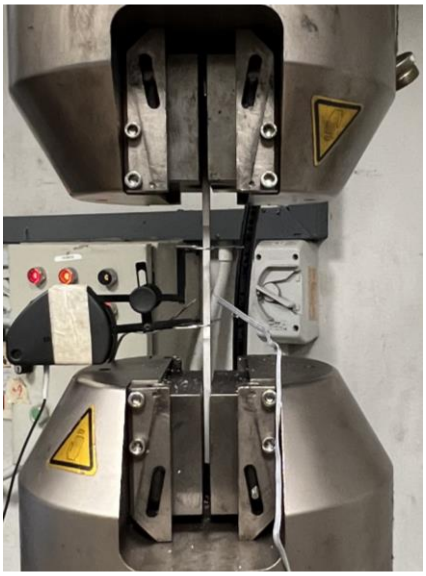

(a) Flat coupon

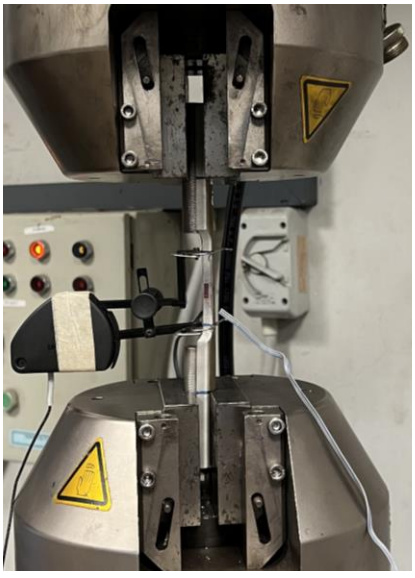

(b) Corner coupon

Fig. 8. Tensile coupon test setup.

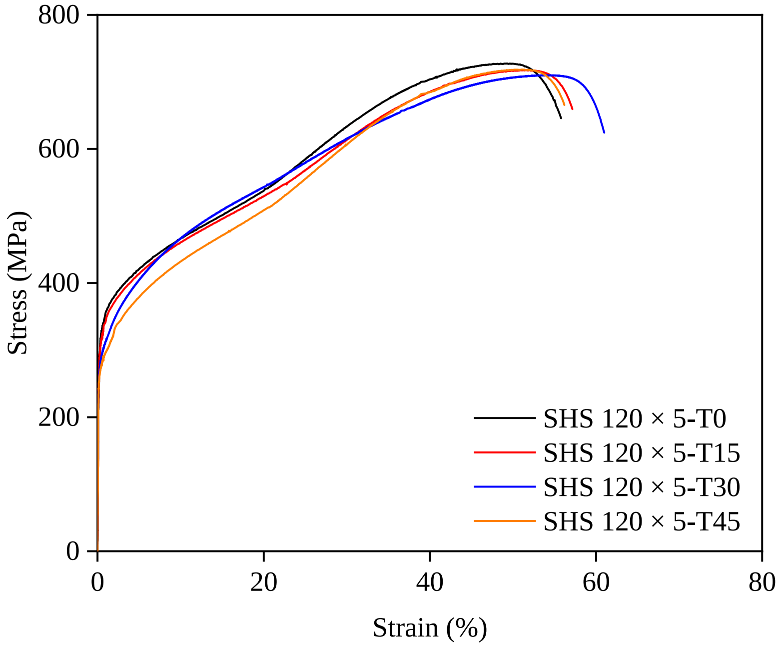

(a) Flat coupons

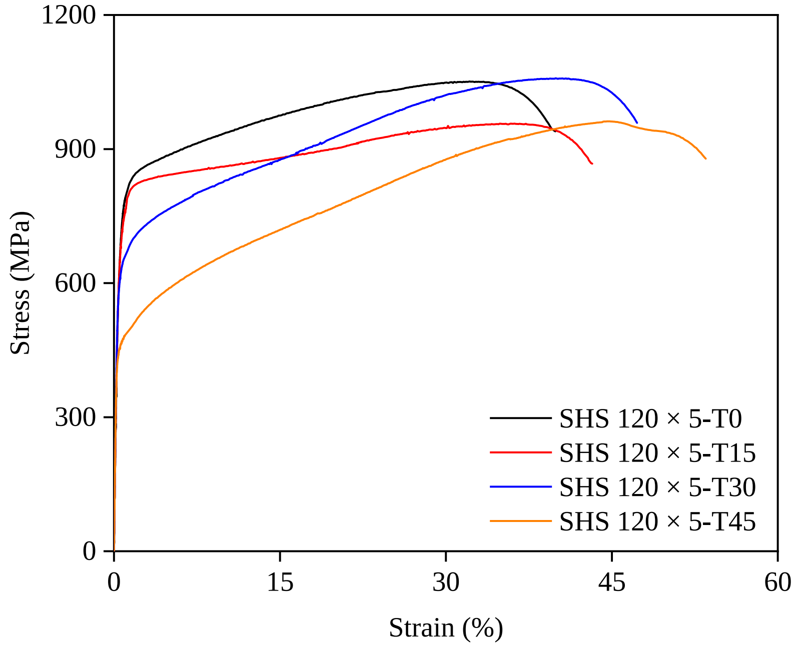

(b) Corner coupons

Fig. 9. Measured ambient temperature and post-fire stress–strain curves of stainless steel tubes.

Fig. 10. Concrete cylinder test setup.

Fig. 11. Stub column test setup.

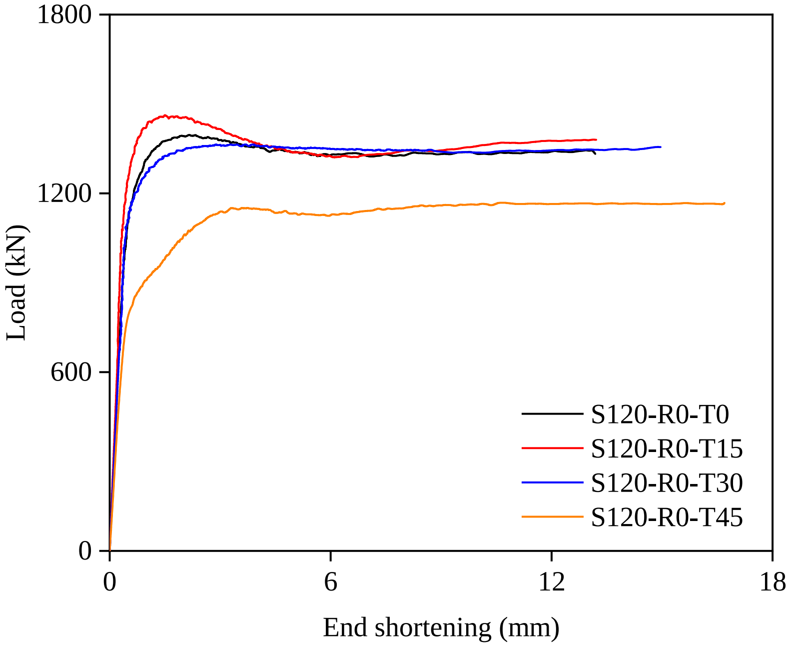

(a) Specimen series S120-R0

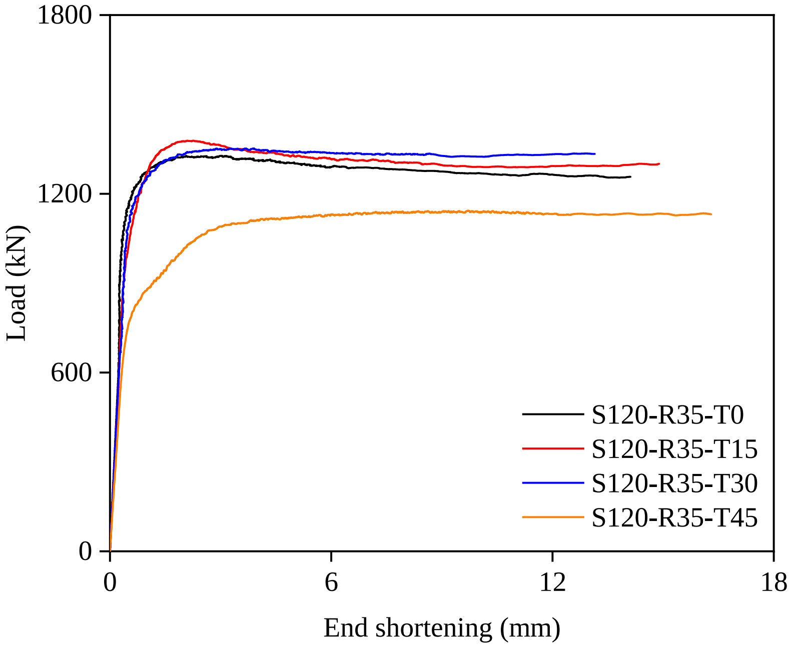

(b) Specimen series S120-R35

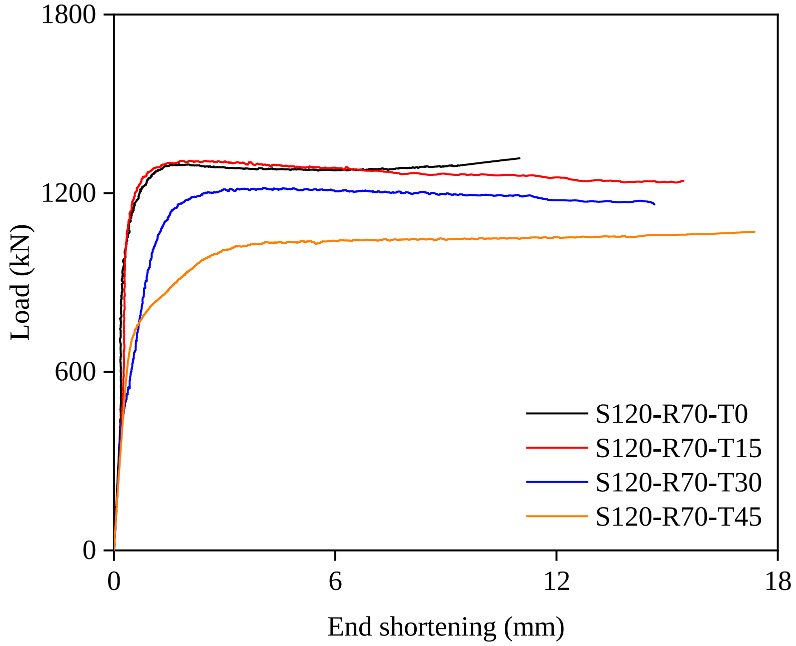

(c) Specimen series S120-R70

Fig. 12. Load–end shortening curves of square RACFSST stub column specimens at ambient temperature and after exposure to fire.

(a) S120-R0-T15

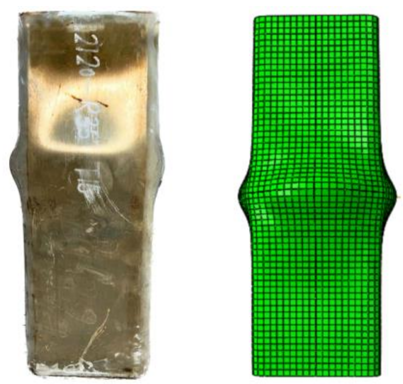

(b) S120-R35-T15

(c) S120-R70-T15

Fig. 13. Experimental and numerical failure modes for typical square RACFSST stub column specimens after exposure to fire.

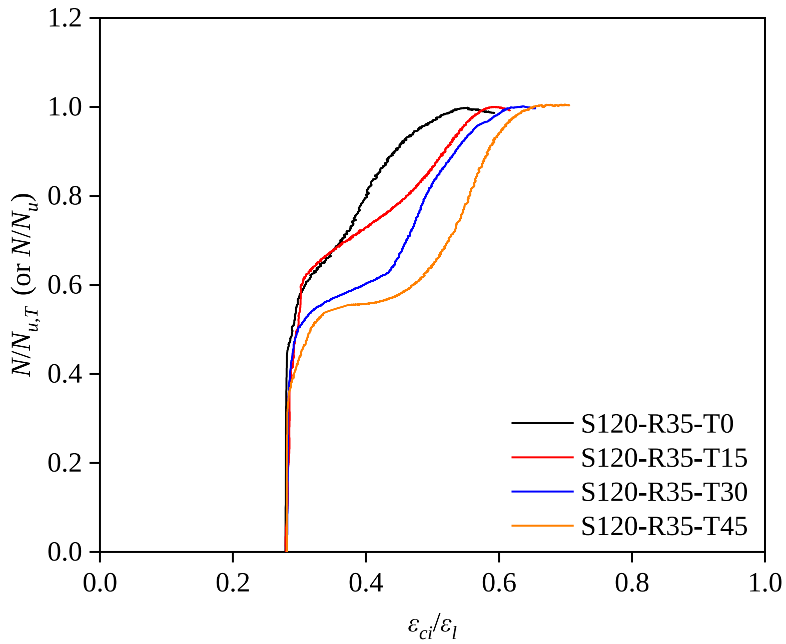

Fig. 14. Development of circumferential-to-longitudinal strain ratios for typical specimen series S120-R35.

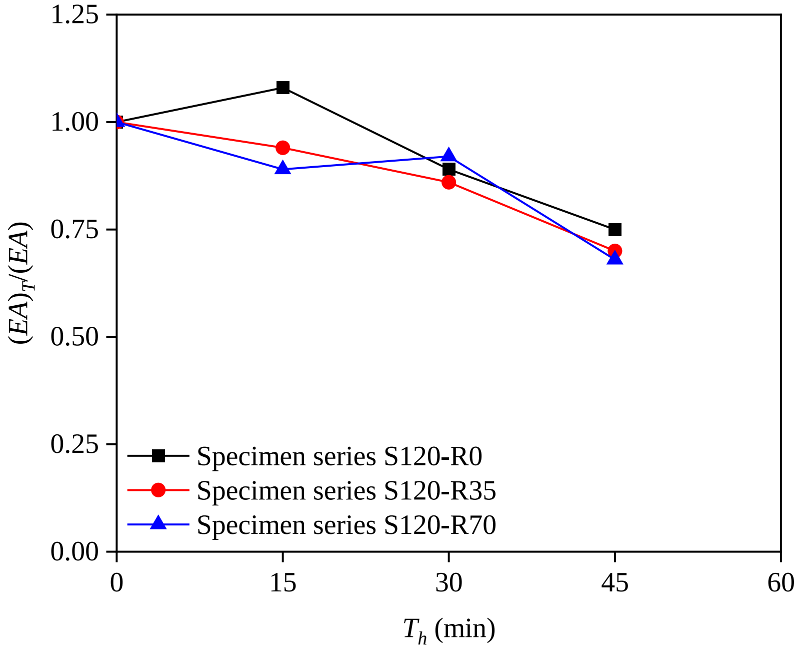

Fig. 15. Influence of heating duration on initial compressive stiffness.

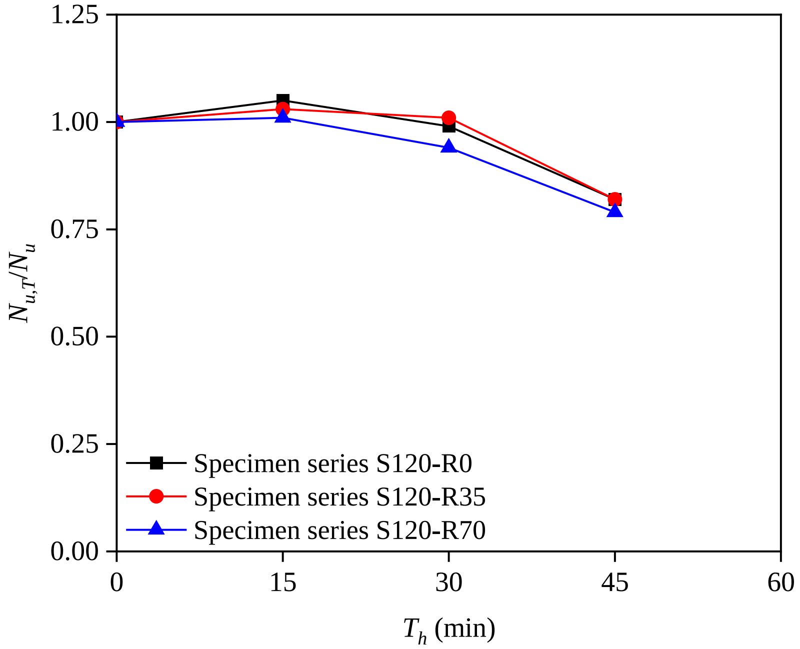

Fig. 16. Influence of heating duration on failure load.

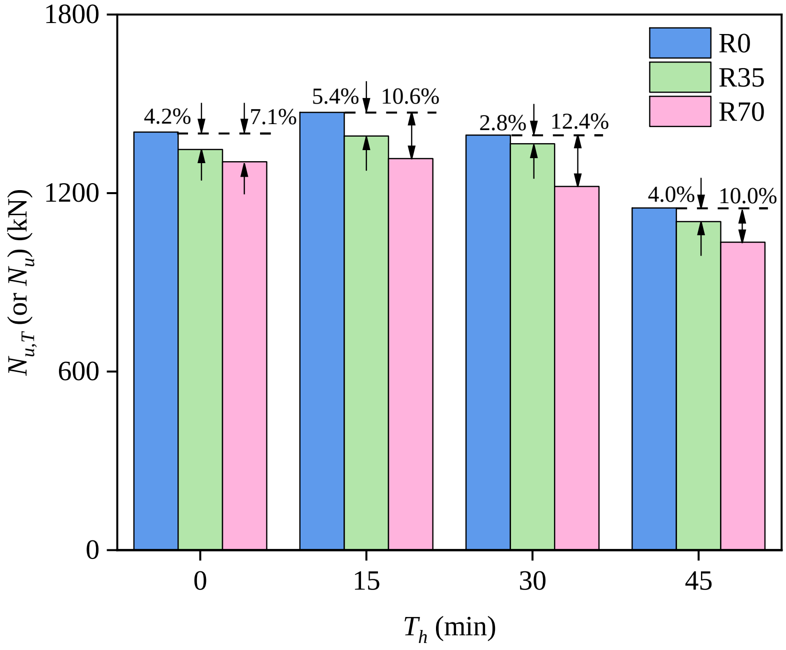

Fig. 17. Influence of RCA replacement ratio on failure load.

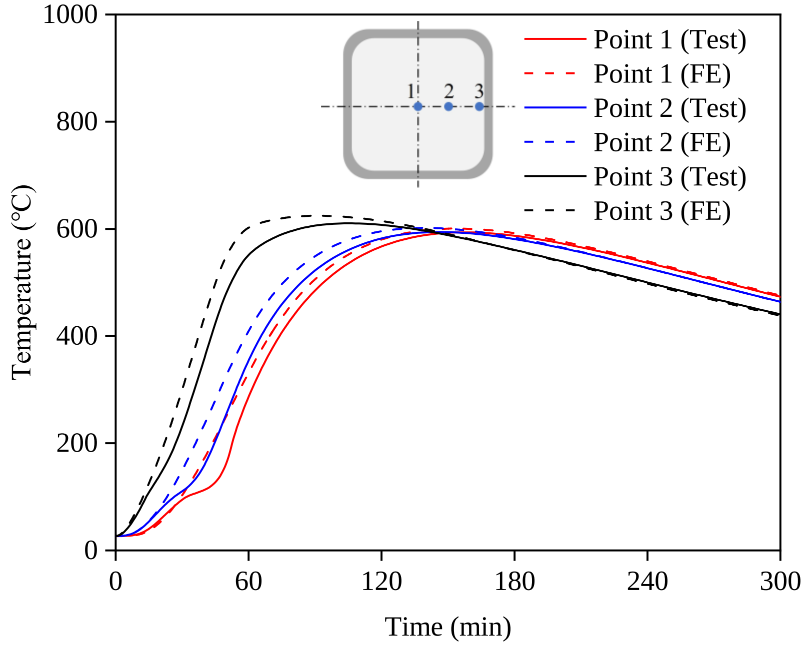

Fig. 18. Comparisons between test and FE temperature–time curves for typical specimen S120-R35-T45.

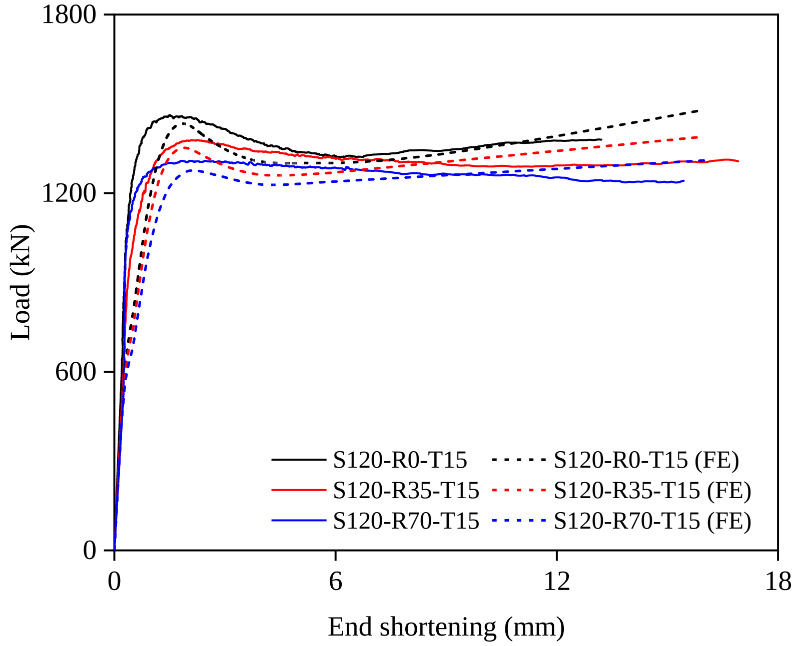

Fig. 19. Comparisons between test and FE load–end shortening curves for typical specimens.

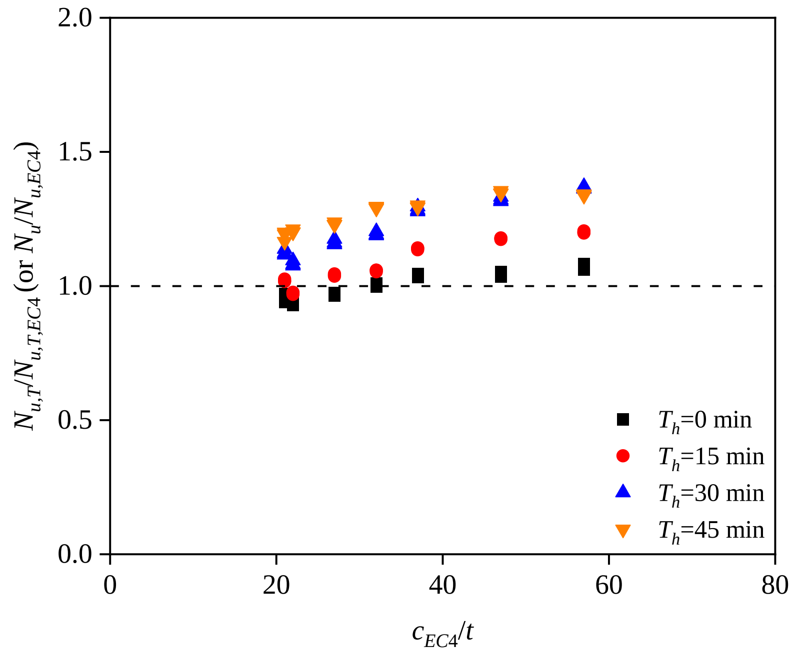

Fig. 20. Comparisons of test and FE failure loads with EC4 predicted failure loads.

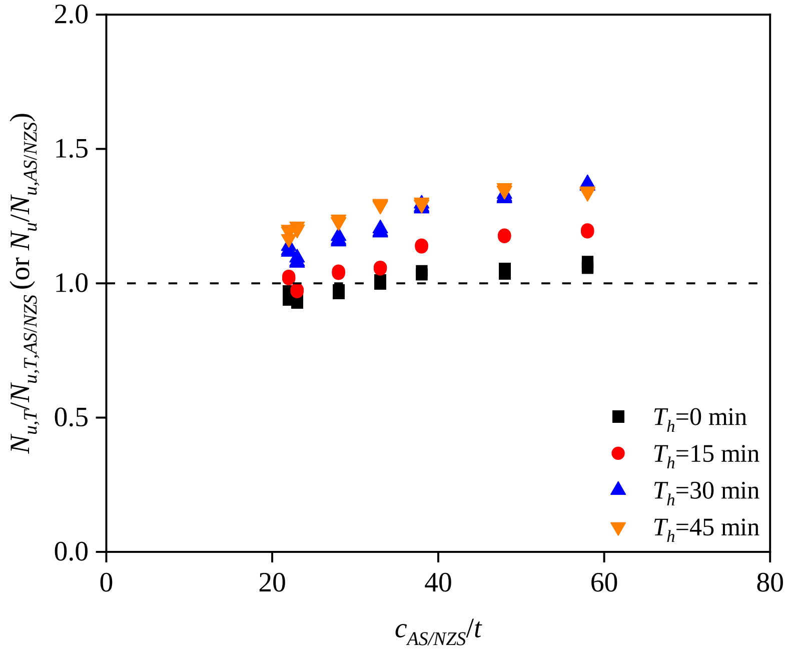

Fig. 21. Comparisons of test and FE failure loads with AS/NZS predicted failure loads.

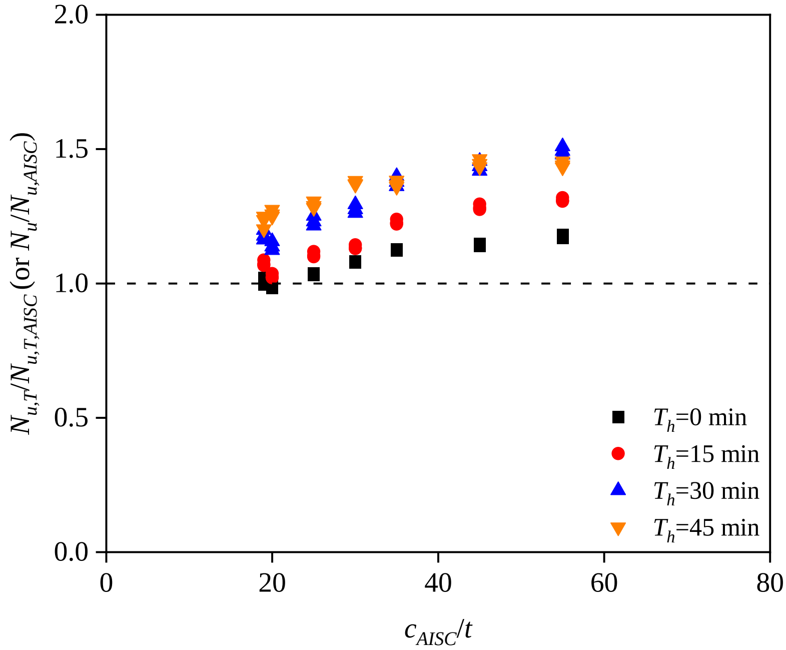

Fig. 22. Comparisons of test and FE failure loads with AISC predicted failure loads.

Table 1 Measured geometric dimensions, RCA replacement ratios and heating durations of square RACFSST stub column specimens.

Specimen ID	*b* (mm)	*h* (mm)	*t* (mm)	r_i (mm)	*L* (mm)	*r* (%)	T_h (min)
S120-R0-T0	120.27	119.83	4.80	7.5	361	0	0
S120-R0-T15	120.49	119.76	4.82	7.5	359	0	15
S120-R0-T30	120.31	119.92	4.81	7.5	358	0	30
S120-R0-T45	120.72	119.71	4.84	7.5	360	0	45
S120-R35-T0	120.21	119.91	4.81	7.5	360	35	0
S120-R35-T15	120.75	119.69	4.78	7.5	358	35	15
S120-R35-T30	120.48	119.82	5.05	7.5	359	35	30
S120-R35-T45	120.77	119.75	5.06	7.5	359	35	45
S120-R70-T0	120.60	119.68	4.81	7.5	359	70	0
S120-R70-T15	120.58	119.72	4.73	7.5	360	70	15
S120-R70-T30	120.13	119.95	4.80	7.5	358	70	30
S120-R70-T45	120.84	119.64	4.81	7.5	360	70	45

Table 2 Physical properties of natural and recycled coarse aggregates.

Type	Loose bulk density (g/cm^3)	Apparent particle density (g/cm^3)	Water absorption ratio (%)
5–20 mm NCA	1.42	2.74	0.74
8 mm NCA	1.36	2.68	1.02
20 mm RCA	1.19	2.58	4.84

Table 3 Requirements for Grading Category G_C80/20 in BS EN 12620.

Sieve size (mm)	Percentage passing by mass (%)
2	0–5
6.3	0–20
20	80–99
31.5	98–100
40	100

Table 4 Mixture proportions of three types of concretes.

Concrete type	Mixture proportion (relative to the weight of cement)						
	5–20 mm NCA	8 mm NCA	20 mm RCA	Sand	Cement	Water	Additional water
R0	1.14	0.49	0.00	1.63	1.00	0.48	0.00
R35	0.58	0.49	0.58	1.63	1.00	0.48	0.03
R70	0.00	0.50	1.16	1.63	1.00	0.48	0.06

Table 5 Measured maximum temperatures for each heating duration.

T_h (min)	T_1 (℃)	T_2 (℃)	T_3 (℃)	T_4 (℃)
15	234.3	234.6	235.7	470.7
30	403.1	403.1	407.4	564.9
45	594.5	598.2	615.9	819.8

Table 6 Measured material properties of stainless steel tubes.

(a) At ambient temperature

Coupon type	T_h (min)	T_4 (℃)	E (MPa)	$\sigma_{0.2}$ (MPa)	σ_u (MPa)	ε_u (%)	ε_f (%)	n	m
Flat	0	30.0	200812	313.1	727.5	49.3	61.6	5.6	2.2
Corner	0	30.0	195320	658.5	1051.4	32.4	39.4	2.8	2.8

(b) After exposure to fire

Coupon type	T_h (min)	T_4 (℃)	E_T (MPa)	$\sigma_{0.2,T}$ (MPa)	$\sigma_{u,T}$ (MPa)	$\varepsilon_{u,T}$ (%)	$\varepsilon_{f,T}$ (%)	n_T	m_T
Flat	15	470.7	203316	307.4	717.6	52.1	64.0	10.2	2.2
	30	564.9	201530	280.6	710.2	54.0	67.8	7.9	2.1
	45	819.8	200640	269.1	718.6	51.2	69.6	15.9	2.1
Corner	15	470.7	193598	646.6	956.9	36.4	44.2	3.9	2.9
	30	564.9	192783	600.5	1058.4	40.1	49.8	6.6	2.6
	45	819.8	193029	444.5	964.5	46.2	61.4	11.2	2.3

Table 7 Measured material properties of three types of concretes at ambient temperature.

Concrete type	$f_{c,28}$ (MPa)	f_c (MPa)	E_{cm} (MPa)
R0	42.1	50.9	32834
R35	37.2	44.3	30244
R70	30.9	36.7	27419

Table 8 Summary of test and FE results of square RACFSST stub column specimens.

(a) At ambient temperature

Specimen ID	N_u (kN)	δ_u (mm)	EA ($\times 10^4$ kN)	FE N_u/Test N_u
S120-R0-T0	1405.1	1.97	92.61	1.02
S120-R35-T0	1346.3	2.07	93.29	1.00
S120-R70-T0	1305.1	1.66	86.55	0.98

(b) After exposure to fire

Specimen ID	$N_{u,T}$ (kN)	$\delta_{u,T}$ (mm)	$(EA)_T$ ($\times 10^4$ kN)	$N_{u,T}/N_u$	$(EA)_T/(EA)$	FE $N_{u,T}$/Test $N_{u,T}$
S120-R0-T15	1471.3	1.35	99.84	1.05	1.08	0.98
S120-R0-T30	1394.9	2.56	82.77	0.99	0.89	1.02
S120-R0-T45	1149.9	3.88	69.48	0.82	0.75	1.04
S120-R35-T15	1391.7	2.38	87.33	1.03	0.94	0.97
S120-R35-T30	1365.6	2.89	80.11	1.01	0.86	0.98
S120-R35-T45	1104.3	4.03	65.01	0.82	0.70	1.03
S120-R70-T15	1315.7	2.60	76.64	1.01	0.89	0.97
S120-R70-T30	1222.2	4.09	79.29	0.94	0.92	1.03
S120-R70-T45	1034.9	4.79	58.46	0.79	0.68	1.04

Table 9 Comparisons between test and FE maximum temperatures.

T_h (min)	FE T_1/Test T_1	FE T_2/Test T_2	FE T_3/Test T_3
15	1.09	1.10	1.15
30	1.04	1.05	1.07
45	1.01	1.01	1.02

Table 10 Outer stainless steel tube dimensions, inner concrete types and heating durations selected for parametric studies.

h (mm)	b (mm)	t (mm)	r_i (mm)	h/t	T_h (min)	Concrete type
120	120	2.00	3.00	60	0, 15, 30, 45	R0, R35, R70
120	120	3.00	4.50	40	0, 15, 30, 45	R0, R35, R70
150	150	3.00	4.50	50	0, 15, 30, 45	R0, R35, R70
150	150	5.00	7.50	30	0, 15, 30, 45	R0, R35, R70
200	200	5.71	8.57	35	0, 15, 30, 45	R0, R35, R70
200	200	8.00	12.00	25	0, 15, 30, 45	R0, R35, R70

Table 11 Comparisons of test and FE failure loads with predicted failure loads.

T_h (min)	No. of test data	No. of FE data	$N_{u,T,}/N_{u,T,EC4}$ (or $N_u/N_{u,EC4}$)		$N_{u,T}/N_{u,T,AS/NZS}$ (or $N_u/N_{u,AS/NZS}$)		$N_{u,T}/N_{u,T,AISC}$ (or $N_u/N_{u,AISC}$)	
			Mean	COV	Mean	COV	Mean	COV
0	3	18	1.00	0.05	1.00	0.05	1.08	0.06
15	3	18	1.09	0.07	1.09	0.07	1.17	0.09
30	3	18	1.22	0.08	1.22	0.08	1.31	0.10
45	3	18	1.27	0.05	1.27	0.05	1.35	0.06
Total	12	72	1.14	0.11	1.14	0.11	1.22	0.12